INSTITUTE OF PHYSICS PUBLISHING JOURNAL OF PHYSICS D: APPLIED PHYSICS

J. Phys. D: Appl. Phys. **36** (2003) 3156–3167 PII: S0022-3727(03)65940-1

A similarity parameter for capillary flows

K A Polzin and E Y Choueiri

Electric Propulsion and Plasma Dynamics Laboratory (EPPDyL), Mechanical and Aerospace Engineering Department, Princeton University, Princeton, New Jersey 08544, USA

E-mail: choueiri@princeton.edu

Received 11 July 2003
Published 25 November 2003
Online at stacks.iop.org/JPhysD/36/3156

Abstract

A similarity parameter for quasi-steady fluid flows advancing into horizontal capillary channels is presented. This parameter can be interpreted as the ratio of the average fluid velocity in the capillary channel to a characteristic velocity of quasi-steady capillary flows. It allows collapsing a large data set of previously published and recent measurements spanning five orders of magnitude in the fluid velocity, 14 different fluids, and four different geometries onto a single curve and indicates the existence of a universal prescription for such flows. On timescales longer than the characteristic time it takes for the flow to become quasi-steady, the one-dimensional momentum equation leads to a non-dimensional relationship between the similarity parameter and the penetration depth that agrees well with most measurements. Departures from that prescription can be attributed to effects that are not accounted for in the one-dimensional theory.

This work is dedicated to Professor Harvey Lam on the occasion of his recovery.

1. Introduction

1.1. Historical perspective

The first analytical studies of surface tension and capillarity were by Young [1] and Laplace [2]. Working independently at approximately the same time, both stated that at a liquid/vapour interface the difference between the liquid's pressure, p_l, and the vapour's pressure, p_v, is proportional to the total curvature of the interface itself. For a spherical meniscus, this can be written as

$$p_v - p_l = \frac{2\gamma}{R}\cos\theta, \tag{1}$$

where γ is the surface tension, θ is the contact angle, and R is the radius of the interface.

Hagen [3] and Poiseuille [4] later studied the flow of viscous liquids in circular pipes (including capillary tubes) and derived an equation for the steady-state volume flow rate based on the radial velocity profile for a fully developed flow (Hagen–Poiseuille flow) given by

$$u(r) = \frac{1}{4\mu}\frac{\Delta p}{\Delta x}(a^2 - r^2), \tag{2}$$

where Δp is the total pressure drop in a column of fluid of length Δx, μ is the viscosity, and a is the tube radius. Reynolds experimentally tested the stability of this profile, finding that it held for laminar flows [5].

At the beginning of the 20th century, there were several works concerned with the dynamics of fluid penetration into capillary tubes [6–10]. One of the results of these studies is the derivation of the Washburn equation for laminar fluid penetration into a horizontal capillary [9]. In the derivation it is assumed that the pressures at the tube inlet ($x = 0$) and in the air beyond the meniscus are equal. The pressure drop, Δp, over the length of the tube is time-independent and is given by equation (1) for a circular tube. If the flow is fully developed and quasi-steady, then the velocity profile is given by equation (2), where Δx is replaced by the variable meniscus position, x_*, representing the distance the fluid penetrates into the tube in time t. Averaging over the velocity profile and integrating in time yields

$$x_*^2 = \frac{\Delta p a^2}{4\mu}t. \tag{3}$$

There have since been several decades of research on dynamic capillary phenomena such as surface wetting and droplet spreading by capillary action. Included in this research have been attempts to reconcile the no-slip boundary condition of continuum fluid mechanics with the condition of contact line motion. Comprehensive reviews of capillary dynamics research can be found in [11–13] and more recent work on reconciling the no-slip condition is discussed by Cox [14] and Bertozzi [15].

Recently, there have been many experimental and theoretical studies on the one-dimensional spreading rates of liquids flowing horizontally under capillary action. For example, liquids have been studied flowing in thin tubes [16], in surface grooves [17–21] and on microstrips [22]. All of these systems have been observed to follow Washburn-type dynamics, meaning the flow dynamics are functionally similar to equation (3) (i.e. $x_*^2 \propto t$).

1.2. Motivation and organization

While the study of systems adhering to Washburn-type dynamics is a well developed field and several studies have employed non-dimensional analysis to find similarities in capillary flows for specific geometries [23, 24], no satisfactory attempt has yet been made to find non-dimensional similarity parameters capable of collapsing all experimental data for any system adhering to Washburn dynamics onto a single curve. Consequently, capillary spreading data in the literature are typically presented in various dimensional or dimensionless forms, and the values of the relevant variables can be quite disparate, depending on the geometry or fluid tested.

In this paper, we present a non-dimensional similarity parameter that is a combination of the relevant dimensional parameters of this problem. The similarity parameter is equivalent to the ratio of the average fluid velocity and a characteristic velocity, which is shown to be the maximum velocity for a quasi-steady capillary flow. Using the similarity parameter to non-dimensionalize published capillary spreading-rate data, a large set spanning five orders of magnitude in the fluid velocity, nine different fluids, and three different geometries can be collapsed into a single curve.

In addition to applying our non-dimensionalization scheme to data found in the literature, we also present measurements from our experiments on fluids advancing in a composite capillary tube consisting of two different, constant cross-sectional area tubes. Five fluids were tested in this configuration, with the advancing meniscus velocity spanning four orders of magnitude. Non-dimensionalization of these data collapses the set to generally within a little more than one order of magnitude and departures from the non-dimensional prescription can be primarily attributed to effects that are not accounted for in our one-dimensional theoretical description.

The data collapse implies that a universal relation for quasi-steady capillary flows exists. It is shown that the one-dimensional momentum equation recast in terms of the non-dimensional parameter leads to such a universal relation when the timescales are much longer than the characteristic time it takes for the flow to become quasi-steady.

The outline of the rest of this paper is as follows. In section 2, we introduce the similarity parameter that forms the basis of the paper. In section 3, we introduce the different experimental geometries to which the similarity parameter will be applied. Recent and previously published experimental data from these geometries are then presented and reduced to non-dimensional form in section 4 as a means of evaluating the physical importance of the similarity parameter. In section 5, we discuss some physical insight into the problem and the limitations of the similarity parameter's validity. Finally, in section 6, we present and apply a universal scaling relation for these flows.

2. Similarity parameter

For this problem, the relevant dimensional parameters and their units are

$$[\langle u\rangle] = LT^{-1}, \qquad [a] = L, \qquad [x_*] = L,$$

$$[\mu] = ML^{-1}T^{-1}, \qquad [\Delta p] = ML^{-1}T^{-2},$$

where $\langle u\rangle$ is the average fluid velocity and a is a characteristic length (the radius for capillary tubes). The surface tension, while not explicitly included in this list, is implicitly included because the total pressure drop in these systems is a function of the surface tension as well as the geometry of the problem.

The Buckingham Pi theorem states that we should be able to find two independent, dimensionless parameters by combining the above dimensional parameters. Two such independent parameters are the similarity parameter,

$$\Pi = \frac{\langle u\rangle \mu}{a\Delta p} \tag{4}$$

and the non-dimensional length,

$$X = \frac{x_*}{a}. \tag{5}$$

We see that, physically, Π is the ratio of the competing effects of viscosity and the driving pressure, which is a function of the surface tension. We also recognize that Π is similar to the well-known Capillary number, $\mathrm{Ca} = \langle u\rangle\mu/\gamma$. However, by including the total pressure drop in our list of dimensional parameters instead of the surface tension, we can tailor the final form of Π to different geometric configurations.

Note that Π is also equivalent to a ratio of two velocities. Based on this, we can define a characteristic velocity for capillary flows,

$$U_{\mathrm{cap}} = \frac{a\Delta p}{\mu} \tag{6}$$

and rewrite Π as

$$\Pi = \frac{\langle u\rangle}{U_{\mathrm{cap}}}. \tag{7}$$

We shall defer to section 5 an explanation of the physical meaning of U_{cap}.

Had time been added to the list of relevant dimensional parameters, an additional non-dimensional parameter, such as $t\Delta p/\mu$, would need to be added to our list of dimensionless variables. However, as we show in section 4, the collapse of the data is attained without invoking time. We also show, in section 5, that the irrelevance of time is due to the quasi-steady condition prevailing in all the considered flows.

3. Experimental geometries

In this paper, we apply the similarity parameter to data sets from four different geometries (see figure 1). The geometries analysed are: (*a*) a stepped capillary tube, (*b*) a single capillary tube, (*c*) a V-shaped groove, and (*d*) a hydrophilic microstrip. In the following text, we describe each geometry and the experiments that were originally performed and attempt to write Π and X in terms of relevant, measurable variables. We shall find that the parameter that is most difficult to determine in all these cases is the total pressure drop, Δp, over the length of the capillary.

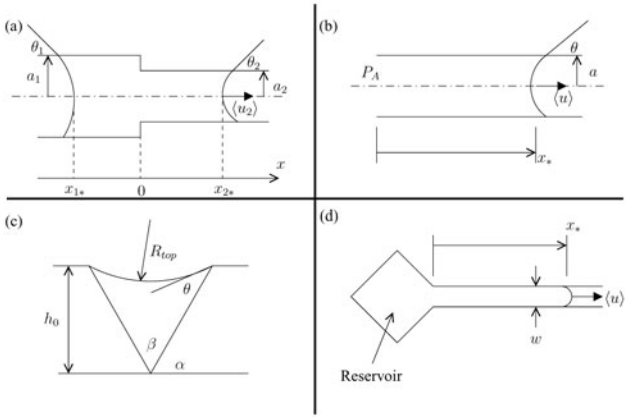

Figure 1. (*a*) A schematic of the stepped capillary tube geometry. (*b*) Schematic of a single tube geometry. (*c*) A view looking along the channel of the V-groove geometry (after [19]). (*d*) A view looking down on the microstrip geometry (after [22]).

3.1. Stepped tube

We conducted experiments using the geometry shown in figure 1(*a*). All quantities with a subscript of 1 denote values in the larger radius tube while the subscript 2 denotes values in the smaller radius tube. The tubes employed were drawn borosilicate glass capillaries with radial tolerances ranging from ±0.05 mm (0.3 mm radius) to ±0.1 mm (1.5 mm radius). The joint between the two different radius capillaries was constructed using epoxy on the flat mating surfaces. A piece of Teflon tubing having a radius approximately equal to the small tube was inserted through both tubes to ensure that when the joint was pressed together epoxy was not forced inwards to form a section possessing a smaller radius than either tube.

We discovered that how the joint is prepared or the roughness of the surface at the joint itself does not matter much, so long as that region is either fully immersed in the liquid (i.e. no liquid/gas/solid interface) or there was not a moving contact line (i.e. trapped air in a crack forming a non-moving liquid/gas/solid interface). To the order of accuracy of our penetration data, this lack of dependence on the preparation of the stepped-tube joint was expected based on the analysis performed both in this section and the appendix, where only moving interfaces are assumed to affect the bulk motion of the fluid.

The capillaries were cleaned by first immersing them in a solution consisting of equal parts H_2O_2(30%) and H_2SO_4 (15 ml each), diluted by 70 ml of deionized water. After being immersed in the solution for 15 min, the capillaries were rinsed by flowing deionized water through them for 2–3 min and then finally blown dry using dry air. The penetration experiments were performed within minutes of completion of the cleaning process.

Initially, fluid was injected into the larger radius tube until the meniscus reached the smaller radius tube. Once the fluid entered the smaller radius tube and fluid completely immersed the joint between the tubes, all active injection was halted. The meniscus position was recorded onto videotape using a camera and VCR. The leading meniscus velocity, $\langle u_2 \rangle \approx \Delta x/\Delta t$, was determined using a standard central-differencing method.

Five different capillary tube radius combinations were tested. These combinations are listed in table 1. In addition to varying the radii, five different fluids were tested, and their properties are given in table 2. The properties for methanol and propanol-2 were taken from [25]. The viscosities and densities of dibutyl phthalate (Sigma-Aldrich Corp., St. Louis, MO) and mechanical and diffusion pump oils (Inland Vacuum Industries, Churchville, NY) were taken from manufacturer data. The listed surface tensions for these three fluids were found by measuring the vertical capillary rise in several different radius tubes while the static contact angles were measured using image analysis. We note that in our computations the static contact angles will always be employed. This is not strictly correct as there is typically some small difference between advancing and receding contact angles (hysteresis, a few degrees for simple liquids [13]). Also, moving contact angles have been observed to differ from their associated static contact angles. However, the moving contact angle is increasingly less sensitive to the flow velocity as the fluid slows [26]. The contact angle enters the non-dimensionalization scheme through the cosine function and since the above effects, in general, introduce only small variations in the similarity parameter, assuming a contact angle equal to the static angle should be an acceptable approximation.

Table 1. Stepped capillary tube radius combinations tested.

	a_1 (mm)	a_2 (mm)
Combination 1	1.50	1.10
Combination 2	1.50	0.60
Combination 3	1.50	0.30
Combination 4	1.35	0.60
Combination 5	1.35	0.30

Table 2. Stepped capillary tube fluids and their properties. The surface tensions and contact angles for the final three fluids were measured by the authors.

Name	γ (mN m^{-1})	μ (mPa s)	ρ (kg m^{-3})	θ (°)
Methanol (CH_4O)	22.1	0.54	790	0
Propanol-2 (C_3H_8O)	20.9	2.04	830	0
Dibutyl phthalate ($C_{16}H_{22}O_4$)	22.3 ± 1.8	20.3	1044	8 ± 4
Fisherbrand 19 Mechanical pump oil	20.8 ± 1.8	47.9	870	22 ± 6
Invoil 940 Si-diffusion pump oil	21.6 ± 2.2	25.9	1070	19 ± 8

To write the non-dimensional parameters, we must first find a solution for the average fluid velocity, $\langle u_2 \rangle$. Taking the pressure gradient, $\mathrm{d}P/\mathrm{d}x$, equal to a constant k in each tube, we can average equation (2) over the cross-sectional area of the tube to obtain an average velocity,

$$\langle u_2 \rangle = \frac{k_2 a_2^2}{8\mu}. \tag{8}$$

An incompressible continuity equation for each radius tube results in the compatibility condition

$$k_1 = \left(\frac{a_2}{a_1}\right)^4 k_2. \tag{9}$$

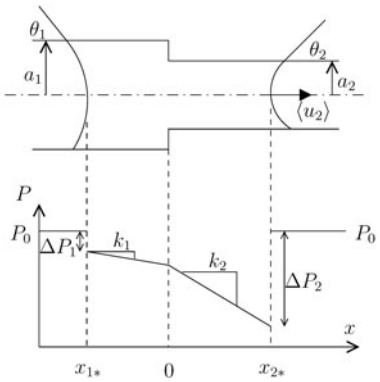

Figure 2. Pressure profile in a stepped capillary tube.

We bring closure to this formulation by assuming a pressure profile in the fluid (see figure 2). The meniscus at each end is exposed to the same outside pressure, and it is known from equation (1) that if the menisci are spherical, the discontinuities in the pressure at each meniscus will be

$$\Delta P_1 = \frac{2\gamma}{a_1}\cos\theta_1, \qquad \Delta P_2 = \frac{2\gamma}{a_2}\cos\theta_2. \tag{10}$$

Using equations (9) and (10) and the fact that the pressure is piecewise continuous between the menisci (see figure 2), analytical expressions for k_1 and k_2 can be found[1]. These are

$$k_1 = \frac{2\gamma(\cos\theta_2/a_2 - \cos\theta_1/a_1)}{x_{2*} - x_{1*}(a_2/a_1)^4}(a_2/a_1)^4, \qquad k_2 = \frac{2\gamma(\cos\theta_2/a_2 - \cos\theta_1/a_1)}{x_{2*} - x_{1*}(a_2/a_1)^4}. \tag{11}$$

In our coordinate system, x_{1*} is measured such that it is always negative and so the denominators in these expressions are always positive.

It is worth noting that the quantity $x_{\mathrm{eq}*}$, which we define as

$$x_{\mathrm{eq}*} \equiv x_{2*} - x_{1*}\left(\frac{a_2}{a_1}\right)^4, \tag{12}$$

has a physical interpretation. It is the length of a column of fluid of radius a_2 and constant pressure gradient k_2 having a pressure drop equal to the total pressure drop between the two menisci. In other words, $|k_2 x_{\mathrm{eq}*}| = |k_1 x_{1*}| + |k_2 x_{2*}|$.

We can now write k_2 as $\Delta p/x_{\mathrm{eq}*}$ and express the similarity parameter (4) as

$$\Pi = \frac{\langle u_2\rangle\mu}{2\gamma}\frac{1}{a_2(\cos\theta_2/a_2 - \cos\theta_1/a_1)} \tag{13}$$

and the dimensionless length (5) as

$$X = \frac{x_{\mathrm{eq}*}}{a_2}, \tag{14}$$

where the radius, a_2, is used as the characteristic length.

[1] Normally, the assumption for the pressure profile at $x \approx 0$ would be that Bernoulli's constant is conserved at the step. However, since the fluid velocities and dynamic pressures in these flows are quite low relative to the static pressure, we can neglect their contributions and assume continuity of static pressure at the step. This can be shown rigorously based upon the analysis performed in section 5.

3.2. Single tube

Fisher and Lark [16] collected data for fluids flowing in thin capillaries. They measured the value of x_*^2/t for different tube radii (see figure 1(*b*)). These experiments were conducted using both water ($\gamma/\mu = 72.7\,\mathrm{m\,s^{-1}}, \theta = 0^\circ$) and cyclohexane ($\gamma/\mu = 22.1\,\mathrm{m\,s^{-1}}, \theta = 8^\circ$) as the working fluid. The goal in that work was to verify the applicability of the Washburn equation (3) for very small tube radii[2].

We see that a single tube is a special case of a stepped capillary tube where $a_1 \to \infty$. Using this fact allows us to simplify the similarity parameter and non-dimensional length given in equations (13) and (14) to

$$\Pi = \frac{\langle u\rangle\mu}{2\gamma}\frac{1}{\cos\theta}, \qquad X = \frac{x_*}{a}. \tag{15}$$

Note that this form assumes the pressure at the immersed end of the tube is equal to the vapour pressure at the fluid/vapour interface (typically atmospheric pressure, P_0). However, as long as the flow can be considered quasi-steady, (15) can be generalized to account for an arbitrary pressure, P_A, at the immersed end. In that case, the pressure difference over the length of the fluid is

$$\Delta p = P_\mathrm{A} - \left[P_0 - \frac{2\gamma\cos\theta}{a}\right]$$

and Π takes on the more general form

$$\Pi = \frac{\langle u\rangle\mu}{2\gamma}\frac{1}{([(P_\mathrm{A} - P_0)a]/(2\gamma) + \cos\theta)}. \tag{16}$$

3.3. V-shaped grooves

For fluids flowing in V-shaped grooves, we use data found in [19]. The geometry that was employed in these experiments (see figure 1(*c*)) consisted of a groove of angle β and height h_0 being fed from a liquid reservoir. Multiple groove angles, groove heights, and liquids were tested, with each test's properties listed in table 3.

A solution for the pressure drop over the length of the groove can be determined using the results of [19]. In that work, the authors found that the governing equation for the spreading could be written as

$$x_*^2 = K(\theta,\alpha)\frac{\gamma h_0}{\mu}t, \tag{17}$$

where the angle α is shown in figure 1(*c*). If we assume that the flow is fully developed and quasi-steady, the velocity profile will have a form similar to that of the Hagen–Poiseuille flow of equation (2) and the flow should follow the Washburn equation (3). Setting $a = h_0$ and comparing equations (17) and (3), it is evident that they are identical if the pressure drop is given by the expression

$$\Delta p = \frac{4\gamma K(\theta,\alpha)}{h_0}. \tag{18}$$

[2] In [16], a velocity-independent contact angle, θ, of 30° for water was assumed for agreement with the Washburn equation. We will not do this in our treatment, opting instead to use the typical water contact angle of $\theta = 0^\circ$.

Table 3. Fluids tested in V-shaped grooves and their properties (after [19]).

Liquid	γ/μ (cm s^{-1})	θ (°)	β (°)	h_0 (μm)	$K(\theta,\alpha)^{1/2}$ Exptl	$K(\theta,\alpha)^{1/2}$ Equation (19)
1,4-Butanediol	59.5	29	45	98.7	0.245	0.282
Cyclohexanol	58.2	6	45	98.7	0.247	0.301
1-Butanol	941	6	45	98.7	0.270	0.301
2-Octanol	408	<2	45	98.7	0.259	0.297
Diethylene glycol	162	33	45	98.7	0.231	0.273
1-Heptanol	489	<2	45	98.7	0.249	0.297
1,4-Butanediol	59.5	29	77	91	0.244	0.219
Cyclohexanol	58.2	6	77	91	0.275	0.248
1-Butanol	941	6	77	91	0.294	0.248
2-Octanol	408	<2	77	91	0.298	0.241
Diethylene glycol	162	33	77	91	0.187	0.204
1-Heptanol	489	<2	77	91	0.281	0.241
Cyclohexanol	58.2	6	124	47.8	0.190	0.174
1-Butanol	941	6	124	47.8	0.194	0.174
2-Octanol	408	<2	124	47.8	0.202	0.166
1-Heptanol	489	<2	124	47.8	0.199	0.166

Several analytical solutions for K have been found [18, 19], each involving a different assumption regarding the radius of curvature of the top surface of the fluid, R_{top} (see figure 1(c)). The solution for K that is generally closest to the experimentally determined value is based on a flat topped fluid ($R_{\text{top}} = \infty$) and is given by

$$K(\theta,\alpha) = \frac{1}{2\pi \sin(\alpha)}\left[\cos(\theta) - \frac{(\alpha-\theta)\cos(\alpha)}{\sin(\alpha-\theta)}\right], \quad (19)$$

where the angle α is shown in figure 1(c). This allows us to write the similarity parameter and dimensionless length for this geometry as

$$\Pi = \frac{\langle u\rangle\mu}{4\gamma}\frac{1}{K(\theta,\alpha)}, \qquad X = \frac{x_*}{h_0}. \quad (20)$$

3.4. Microstrips

Darhuber *et al* [22] conducted experiments using hydrophilic microstrips etched onto a hydrophobic background (see figure 1(d)). The microstrips were connected to a reservoir pad of the same hydrophilic material. A quantity of the working fluid (polydimethylsiloxane silicone oil [Fluka], $\gamma/\mu = 1.03\,\text{m s}^{-1}$) was deposited on the reservoir pad and the fluid then spread along the microstrip through capillary action. In that study it was found that the spreading was governed by an equation similar to (17).

Using the methods of [18], Darhuber *et al* [22] determined for this geometry the variation of their K with the strip width. Unlike the V-shaped grooves, there are no known fully analytical solutions for K in this geometry. However, it was found that the average streamwise velocity should vary according to the relation

$$\langle u\rangle = \frac{K}{2x_*}\frac{\gamma a}{\mu} \propto \frac{\gamma w^4}{\mu}\frac{1}{x_*}, \quad (21)$$

where w is the strip width, which we shall take as the characteristic length scale. To determine Δp for this case, we compare equation (21) with the average fluid velocity of a flow having the velocity profile given by equation (2). Recasting this average velocity in terms of our dimensional variable list and setting $a = w$, we obtain

$$\langle u\rangle = \frac{\Delta p}{x_*}\frac{w^2}{8\mu},$$

which when compared with equation (21) yields

$$\Delta p = \frac{8\gamma w^2}{\zeta}, \quad (22)$$

where we have multiplied the far right-hand side of equation (21) by the proportionality constant ζ^{-1}. We can now write the similarity parameter and dimensionless length as

$$\Pi = \frac{\langle u\rangle\mu}{8\gamma}\frac{\zeta}{w^3}, \qquad X = \frac{x_*}{w}. \quad (23)$$

Note that ζ is a factor with dimensions of length cubed. If equation (22) accurately describes how Δp varies with w and γ, then ζ should be a constant for a given fluid, irrespective of the strip width or surface tension.

4. Experimental data

In this section, we present experimental data for each of the four geometries previously discussed. The literature data will be plotted using the appropriate non-dimensional prescriptions previously developed while the data we present for the stepped capillary tube configuration will first be presented dimensionally and then non-dimensionally. We shall show that, for all cases, the non-dimensional parameter collapses these data, i.e. significantly reduces the range of data spread in one of the variables. The stepped capillary tube data set and discussion will be deferred to the end of this section as an extensive discussion of the data is required.

4.1. Single tube

The penetration data of Fisher and Lark [16] are given in figure 3(a) in coordinates of penetration depth squared per unit time and capillary radius. If the spreading follows equation (3) and the pressure drop is constant, then the value of x_*^2/t should be a constant, $\mathcal{G}$, for a single fluid and tube radius combination. To obtain velocities from these data, we differentiate $x_*^2 = \mathcal{G}t$ to obtain $\mathrm{d}x_*/\mathrm{d}t = \langle u\rangle = \mathcal{G}/2x_*$. For comparing the various data sets, we took $x_* = 50\,\text{mm}$ for all single tube data[3]. The data, non-dimensionalized using equation (15), are replotted in figure 3(b).

[3] The penetration depth for the data set of [16] was not reported in that work. However, it is important to note that whether the penetration depth is taken on the order of 1 or 100 mm, the calculated velocities for this geometry are still bounded by the velocities measured or computed for the other geometries. Hence, the five orders of magnitude collapse in velocity we cite in the abstract is largely independent of the choice of penetration depth for the single tube geometry data.

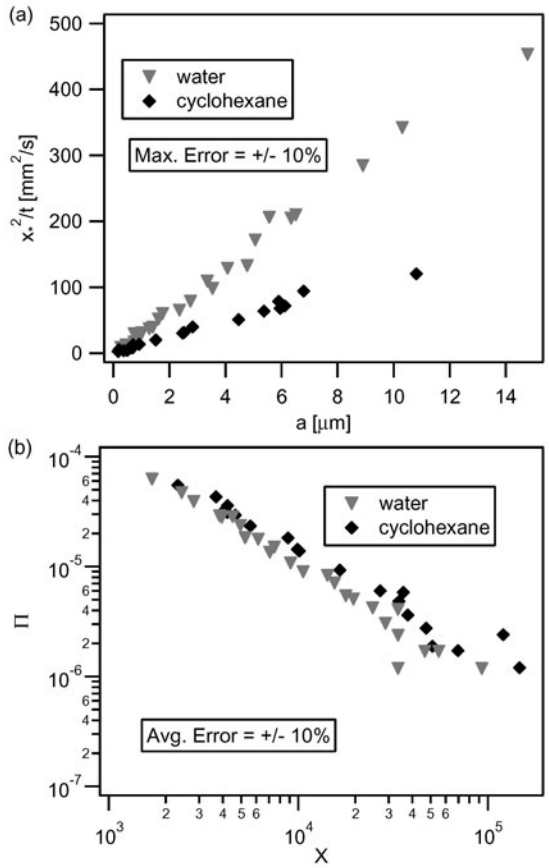

Figure 3. (*a*) Data for fluid penetration rates into a single tube as a function of radius (after [16]). (*b*) The same data plotted using the non-dimensionalization given in equation (15).

We see that the data for both water and cyclohexane do collapse to a single curve. The deviation from this curve at larger values of X is due to the larger relative error in determining the values of x_*^2/t at smaller values of a.

4.2. V*-shaped grooves*

Data sets for fluids flowing into V-shaped grooves are taken from [19] and the fluids tested and their properties are listed in table 3. Included in this table are the values of $K(\theta,\alpha)^{1/2}$ that were computed in [19], where column 6 contains the experimentally determined values and column 7 contains the values computed using equation (19). The data set for $\beta = 45^\circ$ is found in figure 4, the data set for $\beta = 77^\circ$ is found in figures 5(*a*)–(*c*), and the data set for $\beta = 124^\circ$ is found in figures 5(*d*)–(*f*). The velocities were computed in a manner nearly identical to that used for the single tube geometry except that values of x_* need not be assumed as they are explicitly given in the original data set.

We see from the plots in figures 4 and 5 that not only can the data all be collapsed to one curve for each angle β (as Rye *et al* [19] showed), but also that the similarity parameter collapses the data from all groove angles tested to the same curve. Finally, we see that the analytical expression for $K(\theta,\alpha)$, figures 4(*b*), 5(*b*) and (*e*), yields values of Π that are very close to those computed using the experimentally determined values of $K(\theta,\alpha)$, figures 4(*c*), 5(*c*) and (*f*), in

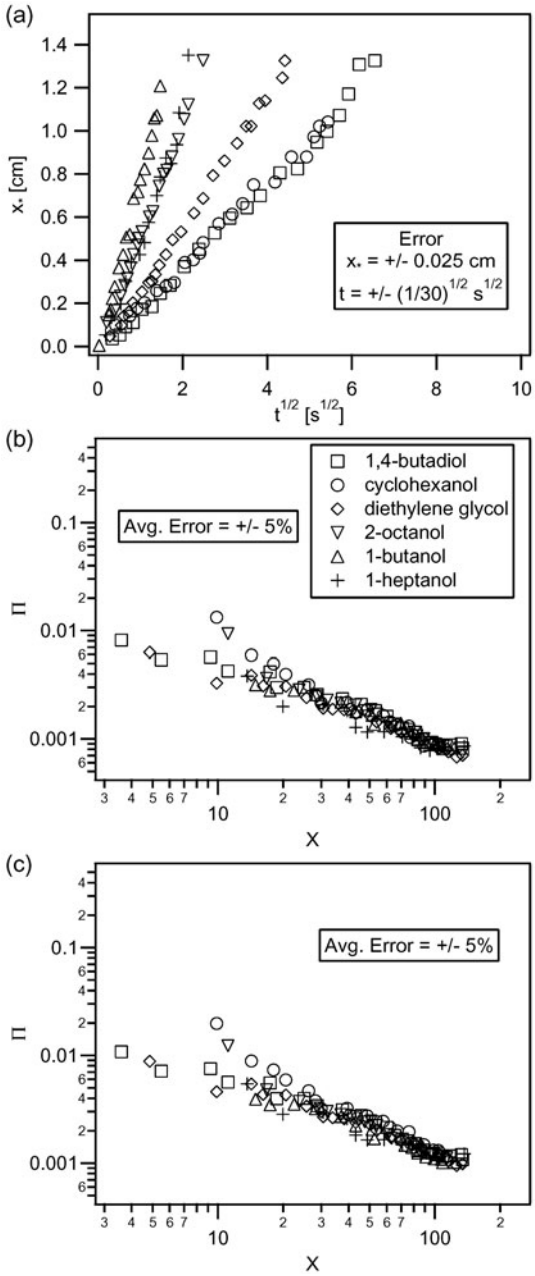

Figure 4. (*a*) Penetration data (after [19]) for fluids flowing in V-shaped grooves cut with an angle $\beta = 45^\circ$. The same data are then replotted using the non-dimensional prescription given in equation (20) with the value of $K(\theta,\alpha)$ (*b*) given in equation (19) and (*c*) computed by Rye *et al* [19] from a curve fit of the experimental data.

all cases, leading us to conclude that equation (19) is a good expression for $K(\theta,\alpha)$.

It is worth mentioning that the collapse of the data in figures 4 and 5 for $X < 10$ is not nearly as good as in the cases where $X > 10$. There are a couple of possible reasons for this. The first is that when $X < 10$, x_* is small and the relative error in knowing its value is larger. Thus, the error bars on the corresponding non-dimensional data are larger. A second reason is that the raw data, plotted in x_* and $t^{1/2}$ coordinates, may be slightly offset (i.e. a straight line curve fit may not exactly pass through zero) due to an initial transient

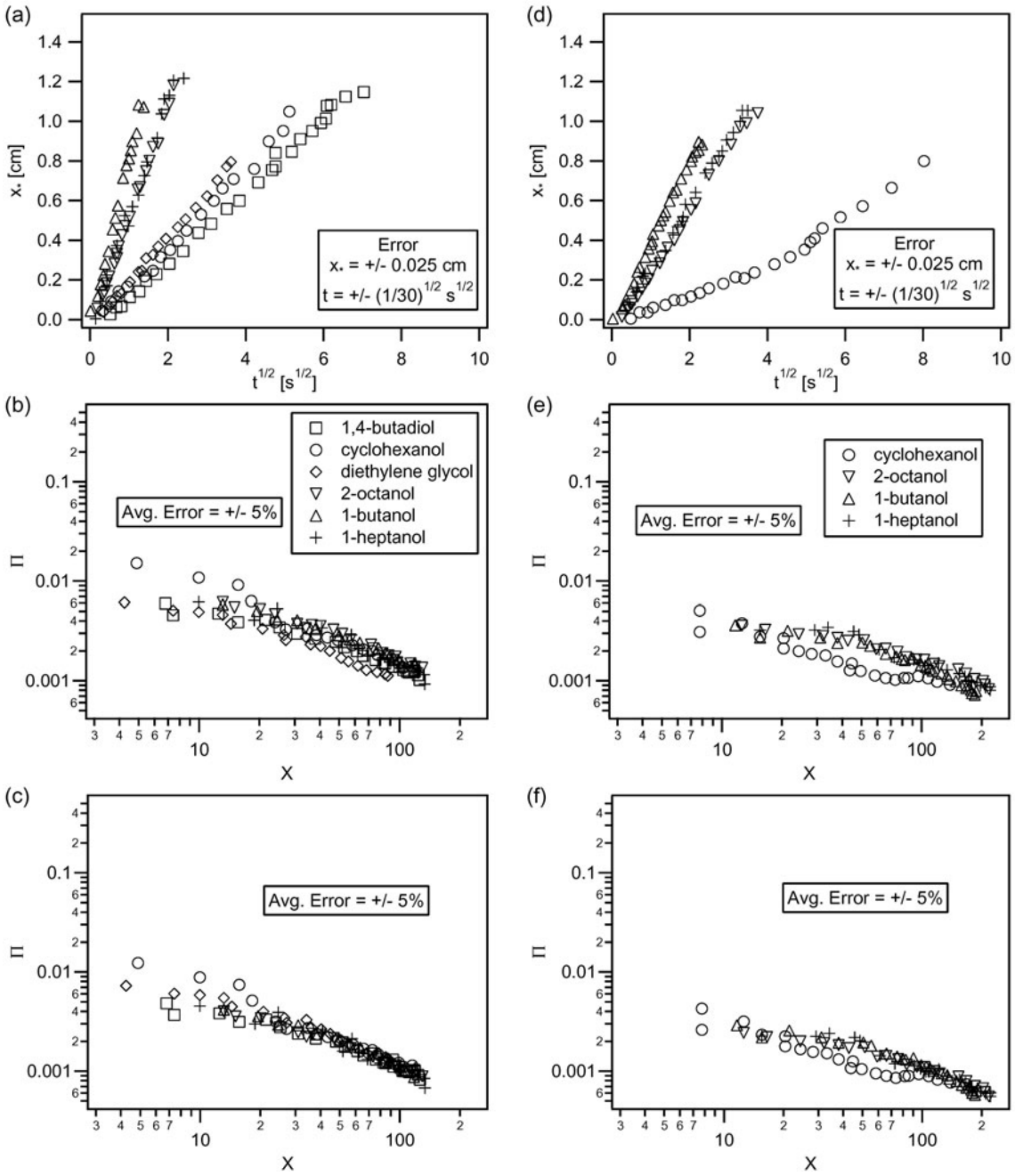

Figure 5. (*a*) Penetration data (after [19]) for fluids flowing in V-shaped grooves cut with an angle $\beta = 77^\circ$. The same data are then replotted using the non-dimensional prescription given in equation (20) with the value of $K(\theta, \alpha)$ (*b*) given in equation (19) and (*c*) computed by Rye *et al* [19] from a curve fit of the experimental data. Analogous data for a groove angle $\beta = 124^\circ$ are given in (*d*)–(*f*).

in the motion of the flow, which could be different for each fluid. A third possibility could be that the flow in this region is not yet quasi-steady, and so our one-dimensional theory and subsequent scaling parameters fail. This possibility will be discussed again in section 5.

4.3. Microstrips

The experimental data for the spreading of liquids on microstrips are taken from [22] and presented in figure 6(*a*). The data set is replotted in figure 6(*b*) using the non-dimensional form given by equation (23). The proportionality constant ζ has been treated as a free parameter in this case. Its value has been chosen such that the data agree with the universal scaling relation presented in section 6. The value of ζ used to non-dimensionalize these data was $5.55 \times 10^{-6}\,\mathrm{m}^3$ or $\zeta^{1/3} = 1.77\,\mathrm{cm}$.

As shown in figure 6(*b*), the data sets for all four widths effectively collapse onto a single curve when our constant ζ is used to compute Π. However, the collapse is independent of the numerical value of ζ, as long as it is a constant for all four widths. This further validates the relevance of both the non-dimensionalization prescribed by equation (23) and the scaling of the velocity given in equation (21).

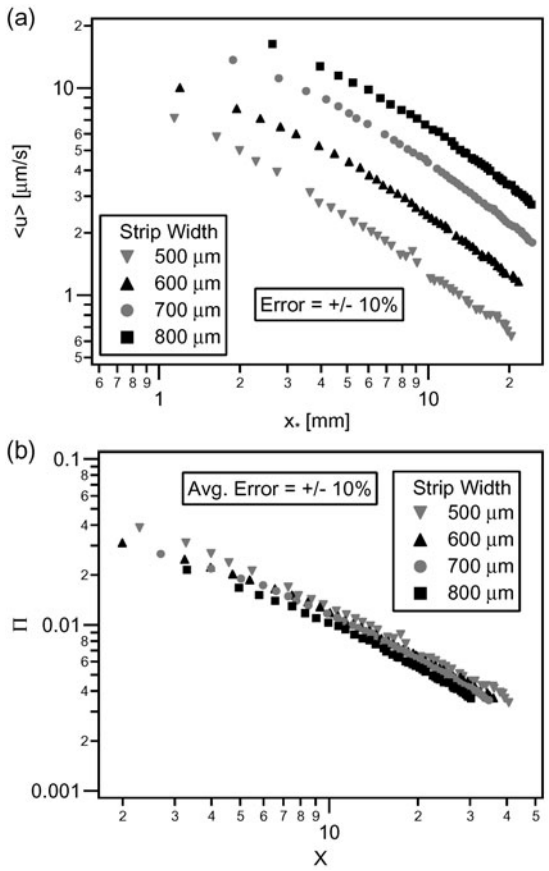

Figure 6. (*a*) Penetration data for polydimethylsiloxane silicone oil flowing on microstrips of varying widths, w (after [22]). (*b*) The same data replotted using the non-dimensionalization given in equation (23), where ζ has been taken equal to $5.55 \times 10^{-6}\,\mathrm{m}^3$ for all widths.

4.4. Stepped tube

Our experimental data for fluids flowing in stepped capillary tubes are shown in figures 7(*a*) and (*b*). These data are divided into two groups, each corresponding to a given radius, a_1 (see figure 1(*a*)). In figures 7(*c*) and (*d*), the data have been non-dimensionalized according to equations (13) and (14).

4.4.1. Discussion of results. We first notice that the dimensional data for the lower viscosity fluids lie virtually on top of each other, while the same data, when recast in the form of the similarity parameter, actually separate. The authors do not know for certain why the dimensional data are aligned in some cases and the corresponding dimensionless data become more poorly aligned. However, we speculate that the advancing contact angles may differ from the static angles given in table 2 due to the higher fluid velocities in those cases and these differences may, in fact, not be the same for different tube radii.

While non-dimensionalizing does collapse the data significantly, the spread is still a little more than an order of magnitude. We especially draw attention to the data corresponding to $a_1 = 1.5\,\mathrm{mm}$ and $a_2 = 1.1\,\mathrm{mm}$. Except for the data for isopropanol these data do not follow the data for any other radius combination. Also, even when the non-dimensionalization is applied, the data do not conform to the other data sets. It may be that the isopropanol tracks the other data sets better because its penetration, due to its greater speed relative to the other data for $a_2 = 1.1\,\mathrm{mm}$, is still predominately governed by a one-dimensional momentum equation like the one employed in section 3.1.

We argue that the data sets that do not track the theory well actually show the usefulness of the similarity parameter. In these cases, we believe that some physical mechanism other than Washburn dynamics is governing the penetration of the fluid. The fact that the different data sets are operating in different physical regimes is clearly demonstrated when the penetration data are plotted in coordinates of Π and X. We shall revisit this point again once we derive a universal relation between the similarity parameter and non-dimensional length.

4.4.2. Alternative physical mechanisms. There are a few possible effects that could be influencing the data in figure 7, especially at the higher values of a_2. The first may be that gravity is introducing two-dimensional effects into the problem. It is convenient for us to use the Bond number, which is defined as the ratio of gravitational to surface tension forces and is written as

$$\mathrm{Bo} = \frac{\rho g d^2}{\gamma},$$

where d is the capillary tube diameter. The values of Bo for tubes possessing radii corresponding to values of a_2 vary between $\mathcal{O}(0.1)$ and $\mathcal{O}(1)$, implying that gravity should play some role in the development of the flow in at least some of the cases.

It is experimentally observed that the meniscus deforms with increasing Bo, as shown schematically in figure 8. This deformation may yield a pressure drop across the mensicus that is no longer given by equation (10). As such, we would fully expect the non-dimensionalization to fail for cases where Bo is close to unity.

A second possibility is that the meniscus is not moving in the assumed steady, continuous fashion, but instead is exhibiting stick–slip motion and contact line pinning as discussed in [27, 28]. It is possible that the higher viscosity, slower moving fluids in our experiments were advancing in this manner and that this resulted in deviations from the one-dimensional theoretical description.

5. Physical insight and limitations

In the appendix, we show that the momentum equation for a flow entering a capillary tube from a semi-infinite reservoir can be written as

$$\frac{B\tau^2}{a^2}\left[\left(x_* + \frac{a}{2}\right)\frac{\mathrm{d}^2 x_*}{\mathrm{d}t^2} + \frac{1}{8}\left(\frac{\mathrm{d}x_*}{\mathrm{d}t}\right)^2\right] = 1 - \frac{x_*\tau}{a^2}\frac{\mathrm{d}x_*}{\mathrm{d}t}. \quad (24)$$

In this equation, τ and B are, respectively, a dimensional timescale and a dimensionless parameter and are defined as

$$\tau = \frac{8\mu}{\Delta p}, \qquad B = \frac{\rho a^2}{\tau^2 \Delta p} = \frac{\rho a^2 \Delta p}{(8\mu)^2}.$$

Also, x_*, $\mathrm{d}x_*/\mathrm{d}t$, and $\mathrm{d}^2x_*/\mathrm{d}t^2$ are, respectively, the position, velocity, and acceleration of the moving air–liquid interface.

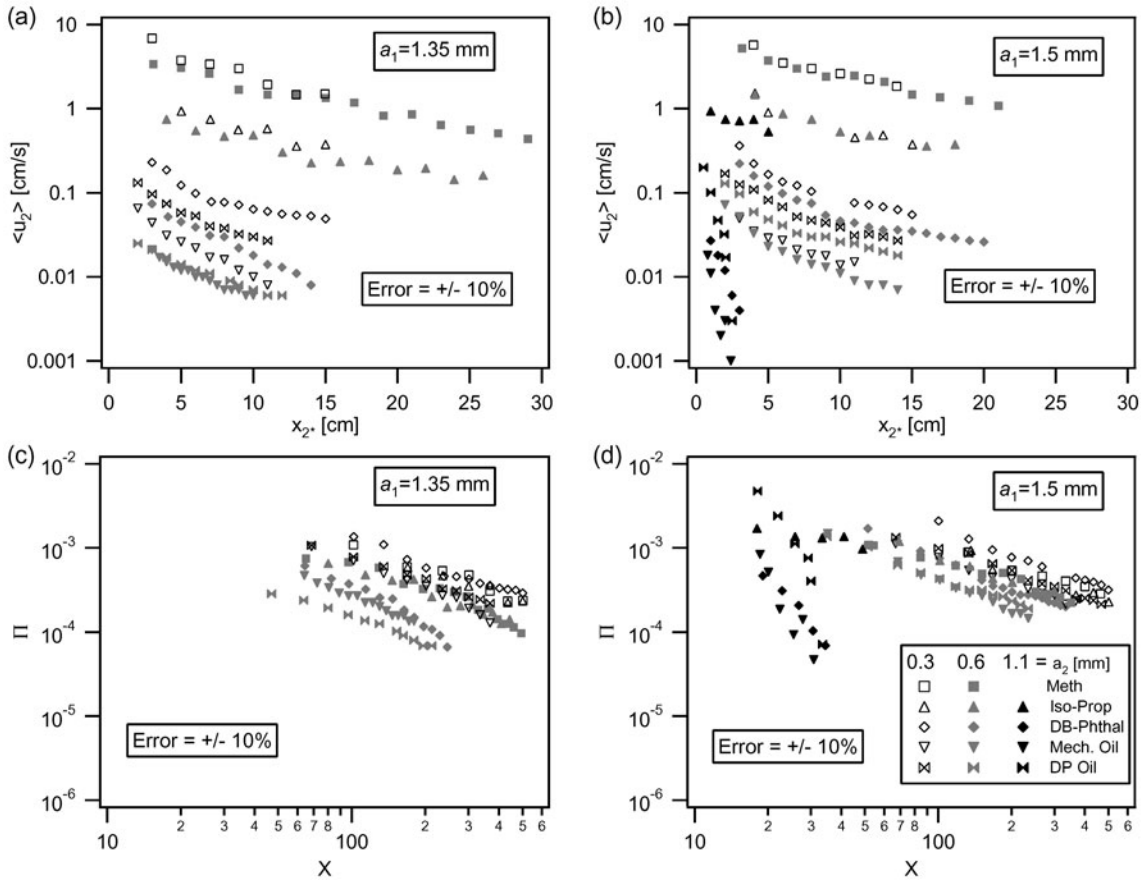

Figure 7. (*a*) and (*b*) Velocity as a function of penetration depth for fluids flowing in stepped capillary tubes (a_1 as noted on the graphs). (*c*) and (*d*) The same data plotted using the non-dimensionalization of equations (13) and (14).

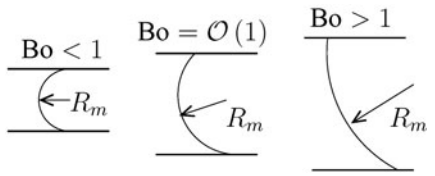

Figure 8. Schematic showing how the meniscus deforms with increasing Bo.

5.1. Dimensionless formulation and solution

Introducing the dimensionless variables X and ξ,

$$X = \frac{x_*}{a}, \qquad \xi = \frac{t}{\tau} = \frac{t\Delta p}{8\mu},$$

we can rewrite equation (24) as

$$B\left[\left(X + \frac{1}{2}\right)\frac{\mathrm{d}^2X}{\mathrm{d}\xi^2} + \frac{1}{8}\left(\frac{\mathrm{d}X}{\mathrm{d}\xi}\right)^2\right] = 1 - X\frac{\mathrm{d}X}{\mathrm{d}\xi}. \tag{25}$$

For problems of interest, the condition $X \geqslant 1$ should be satisfied. We notice that if the left-hand side of equation (25) is negligible, the solution is

$$X = \sqrt{2\xi}, \tag{26}$$

which is the non-dimensional version of the Washburn equation (3).

Consistent with the Washburn solution we have

$$\left(\frac{\mathrm{d}X}{\mathrm{d}\xi}\right)^2 = \frac{1}{2\xi}, \qquad X\frac{\mathrm{d}^2X}{\mathrm{d}\xi^2} = -\frac{1}{2\xi}. \tag{27}$$

For the left-hand side of equation (25) to be negligible, the inequality $B \ll \xi$ must be satisfied. Rewriting this inequality in terms of dimensional parameters, we obtain

$$t_{\mathrm{CO}} \equiv \frac{\rho a^2}{8\mu} \ll t, \tag{28}$$

where t_{CO} is the 'crossover' time. This implies that for the flow to be considered quasi-steady, the time must be much greater than t_{CO}, which is essentially the time it takes for viscous diffusion to travel a distance $\mathcal{O}(a)$.

We now return to the case of the V-groove penetration data where $X < 10$, as found in figures 4 and 5. Equation (26) can be rearranged and used to substitute for t in equation (28). Taking $X = 10$, a quick calculation shows that t_{CO} can, in fact, be greater than 1% of t, implying that the flow in cases where $X < 10$ may not yet be quasi-steady.

5.2. Meaning of U_{cap}

If we operate at a time that satisfies the inequality in equation (28), we can substitute for time using the first equation

in (27). Substituting and rearranging yields the expression

$$2\frac{\rho U_{\rm cap} a}{\mu}\left(\frac{\langle u\rangle}{U_{\rm cap}}\right)^2 = 2{\rm Re}|_{U_{\rm cap}}\Pi^2 \ll 1, \qquad (29)$$

where $\mathrm{Re}|_{U_{\rm cap}}$ is a Reynold's number based on the characteristic velocity, $U_{\rm cap}$. For most practical flows such as those discussed here $\mathrm{Re}|_{U_{\rm cap}} \geqslant \mathcal{O}(1)$.

We know that as $\langle u\rangle \to U_{\rm cap}$, $\Pi \to 1$. When this occurs the inequality in equation (29) is violated and the flow cannot be considered quasi-steady. We conclude that $U_{\rm cap}$ is a characteristic velocity for capillary flows. For times later than $t_{\rm CO}$, the flow becomes quasi-steady, the inequality in equation (29) holds, and the fluid velocity is always less than $U_{\rm cap}$. Since $\langle u\rangle$ is less than $U_{\rm cap}$ for all the developed flows considered in this paper, we conclude that these flows are essentially quasi-steady[4].

6. Scaling relation

In this section, we turn our attention to the problem of finding a relationship between the similarity parameter, Π, and the non-dimensional length, X. For times greater than $t_{\rm CO}$, we can set the left-hand side of equation (25) equal to zero and then rearrange the right-hand side to obtain

$$\frac{{\rm d}X}{{\rm d}\xi} = X^{-1}. \qquad (30)$$

Writing the left-hand side of this equation in terms of the similarity parameter yields the universal relation

$$\Pi = \tfrac{1}{8}X^{-1}. \qquad (31)$$

In figure 9, we have plotted all the literature data presented in this paper using the variables Π and X while the authors' data for a stepped-tube can be found in figure 10. In addition, the line given by equation (31), representing the scaling relation between the non-dimensional parameters, has been plotted in both figures. The first plot shows that not only do all the literature data, independent of geometry or fluid, effectively collapse to a single curve, but that this curve is given by the scaling relation. The second plot shows the increasing failure of the scaling relation to fully collapse the authors' own data as a_2 increases (see figure 7 for the corresponding values of a_2). We again emphasize that this failure should be understood as a crossover between a regime where Washburn dynamics governs the penetration of the fluid and a regime where some other physical effect begins to dominate. The usefulness of plotting data using the similarity parameter and comparing these plots with the universal scaling relationship is that one can unequivocally determine if the flow is governed by Washburn dynamics.

[4] It is interesting to note that the similarity parameter, Π, is analogous to the Crocco number, Cr, of compressible gas dynamics [29], which is also equivalent to a velocity non-dimensionalized by a maximum velocity, $V/V_{\rm max}$. In that case, $V_{\rm max}$ is the maximum velocity a gas can attain when adiabatically expanded to zero temperature.

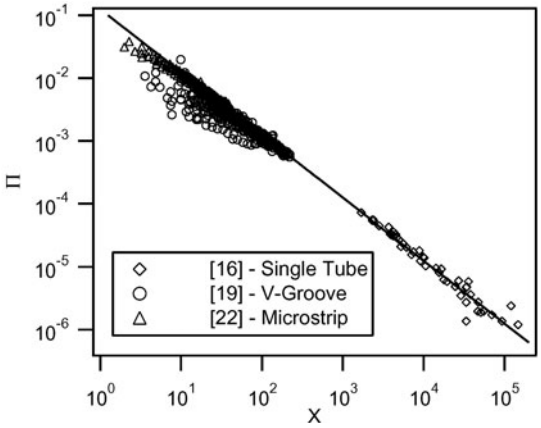

Figure 9. All literature penetration data contained within this paper plotted in coordinates of Π and X. In addition, equation (31), representing the universal scaling relation, is plotted.

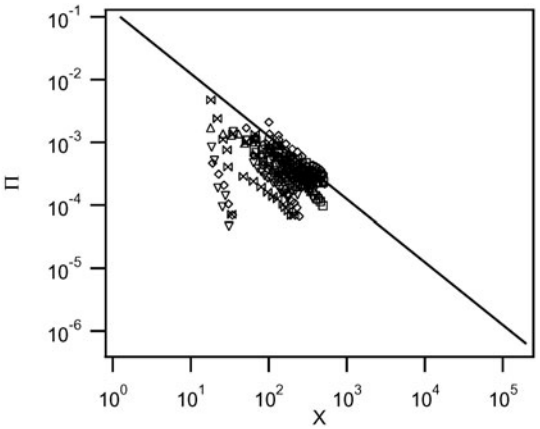

Figure 10. The authors' stepped-tube penetration data plotted in coordinates of Π and X. In addition, equation (31), representing the universal scaling relation, is plotted.

7. Conclusions

This study leads to the following major conclusions.

- A similarity parameter for quasi-steady fluids advancing into horizontal capillaries exists and can be found by combining the relevant dimensional parameters of this problem.
- The similarity parameter consists of the ratio between either the effect of viscosity and that of the driving pressure, or the average fluid velocity and a characteristic capillary velocity, $U_{\rm cap}$. When the time is greater than the 'crossover' time, the characteristic velocity is greater than the fluid velocity.
- The similarity parameter collapses a large data set spanning five orders of magnitude in penetration velocity, 14 different fluids, and four different geometries to a single curve. This implies that a relation between the similarity parameter, $\Pi = \langle u\rangle/U_{\rm cap}$, and the non-dimensional distance, X, exists.
- The equation $\Pi = (\frac{1}{8})X^{-1}$, which holds for fully developed quasi-steady flows (i.e. for times much greater than $\rho a^2/8\mu$), provides a universal scaling relation that

agrees well with the collapsed data set over a large range of experimental parameters.

- A determination of whether or not a fluid's penetration is governed by Washburn dynamics can be made by observing if data plotted in coordinates of Π and X align with the universal scaling relation. In this study, a crossover between different physical regimes can clearly be seen when data from the stepped tube experiments are analysed in this manner.

Acknowledgments

This work has greatly benefited from the insightful comments of Prof. S H Lam. We also acknowledge several discussions with Dr A A Darhuber and Dr P G Felton. Support for Mr K A Polzin is provided by the National Defense Science and Engineering Graduate Fellowship programme.

Appendix. Origin of equation (24)

We proceed with a derivation of equation (24) from first principles.

Appendix A.1. Formulation

Consider a straight, round, semi-infinite tube of radius a. This tube extends in the positive x-direction and it is connected to a much larger radius tube in the negative x-direction. At $t \leqslant 0$, liquid fills the $x \leqslant 0$ side and there is no liquid in the $x > 0$ portion of the tube. At $t > 0$, liquid is expected to enter the narrow tube. The static pressures at $x = \pm\infty$ are identical and denoted by p_0. The static pressure on the liquid side of the liquid–air interface is reduced by the surface tension and is given by equation (1). For the moment, we shall take the pressure reduction due to surface tension to be equal to Δp. Let x_* denote the location of the moving air–liquid interface and $\langle u\rangle$ denote its average velocity, or

$$\langle u\rangle = \frac{\mathrm{d}x_*}{\mathrm{d}t}, \qquad 0 \leqslant x \leqslant x_*, \quad t \geqslant 0. \tag{A1}$$

Note that we can rewrite the parabolic velocity profile, equation (2), as

$$u(r) = 2\langle u\rangle\left(1 - \frac{r^2}{a^2}\right). \tag{A2}$$

Appendix A.2. Static pressure at $x \approx 0$

The liquid at $x < 0$ converges and flows towards the entrance of the narrow tube. The static pressure at $x \approx 0$ is less than p_0. For the region where $x < 0$, we can use Bernoulli's equation for an inviscid, unsteady flow,

$$p_0 = p + \rho\left(\frac{V^2}{2} + \frac{\partial\phi}{\partial t}\right) = \text{constant}, \tag{A3}$$

where ϕ is the velocity potential defined as

$$\boldsymbol{V} = \nabla\phi \tag{A4}$$

and $\boldsymbol{V}$ is the liquid velocity vector of magnitude V. Equating the flowrate into the narrow tube with the flowrate through any tube cross-section, we can find a simple sink velocity potential,

$$\phi = \frac{\langle u\rangle a^2}{2r}, \tag{A5}$$

where r is the radial spherical coordinate. We can now evaluate equation (A3) at $x \approx 0$ as

$$p(x \approx 0) = p_0 - \rho\left(\frac{1}{8}\left(\frac{\mathrm{d}x_*}{\mathrm{d}t}\right)^2 + \frac{a}{2}\frac{\mathrm{d}^2x_*}{\mathrm{d}t^2}\right), \tag{A6}$$

where the dynamic pressure and unsteady term in equation (A3) were evaluated at $r = a$. The time-dependent pressure gradient in the narrow tube is expected to be a constant with respect to x. This can be computed by

$$\begin{aligned}\frac{\partial p}{\partial x} &= \frac{(p_0 - \Delta p) - p(x \approx 0)}{x_*},\\ &= -\frac{\Delta p}{x_*} + \frac{\rho}{x_*}\left(\frac{1}{8}\left(\frac{\mathrm{d}x_*}{\mathrm{d}t}\right)^2 + \frac{a}{2}\frac{\mathrm{d}^2x_*}{\mathrm{d}t^2}\right).\end{aligned} \tag{A7}$$

Appendix A.3. x-Momentum equation

The x-momentum equation in the narrow tube is

$$\rho\frac{\partial\langle u\rangle}{\partial t} = -\frac{\partial p}{\partial x} + \mu\nabla^2 u(r). \tag{A8}$$

Taking $u(r)$ to be given by equation (A2), we can rewrite the momentum equation as

$$\rho\frac{\partial\langle u\rangle}{\partial t} = -\frac{\partial p}{\partial x} - \frac{8\mu\langle u\rangle}{a^2}. \tag{A9}$$

Substituting equation (A7) for the pressure gradient and rearranging, we obtain

$$\frac{B\tau^2}{a^2}\left[\left(x_* + \frac{a}{2}\right)\frac{\mathrm{d}^2x_*}{\mathrm{d}t^2} + \frac{1}{8}\left(\frac{\mathrm{d}x_*}{\mathrm{d}t}\right)^2\right] = 1 - \frac{x_*\tau}{a^2}\frac{\mathrm{d}x_*}{\mathrm{d}t}, \tag{A10}$$

where we have defined a dimensional timescale, τ, and a dimensionless parameter, B, as

$$\tau = \frac{8\mu}{\Delta p}, \qquad B = \frac{\rho a^2}{\tau^2\Delta p} = \frac{\rho a^2\Delta p}{(8\mu)^2}.$$

Equation (A10) is exactly equation (24).

We assumed a velocity profile in the derivation of equation (A10) and then performed a 'momentum integral' type analysis. It is interesting to note that our result recovers the form of the governing equation derived using an energy balance formulation by Szekely *et al* [30] but differs on two coefficients (one on the $\mathrm{d}^2x_*/\mathrm{d}t^2$ term and the other on the $(\mathrm{d}x_*/\mathrm{d}t)^2$ term).

The other, implicit assumption we make in introducing the inviscid Bernoulli equation (A3) is that the flow Reynolds number is low. The unsteady terms arising in the x-momentum equation as a result of using the inviscid Bernoulli equation are not reliable except in their order of magnitude (the same is true of the result in [30]). However, we are only interested in the upper bound on these unsteady terms. The useful result of this derivation is the condition under which the neglect of the unsteady terms is justified.

References

[1] Young T 1805 *Phil. Trans. R. Soc.* **95** 65–87
[2] Laplace P S 1966 *Celestial Mechanics* vol IV (English Transl. *Traité de Mécanique Céleste* IV (1805)) (New York: Chelsea) pp 695–712
[3] Hagen G 1839 *Pogg. Ann.* **46** 423–42
[4] Poiseuille J 1840 *C. R. Acad. Sci.* **11** 961–1041
[5] Reynolds O 1883 *Phil. Trans. R. Soc.* **174** 935–82
[6] Bell J M and Cameron F K 1906 *J. Phys. Chem.* **10** 658–74
[7] West G D 1911 *Proc. R. Soc. Lond. Ser.* A **86** 20–5
[8] Cude H E and Hulett G A 1920 *J. Am. Chem. Soc.* **42** 391–401
[9] Washburn E W 1921 *Phys. Rev.* **17** 273–83
[10] Rideal E K 1921 *Phil. Mag.* **44** 1152–9
[11] Dussan E B 1979 *Ann. Rev. Fluid Mech.* **11** 371–400
[12] de Gennes P G 1985 *Rev. Mod. Phys.* **57** 827–63
[13] Leger L and Joanny J F 1992 *Rep. Prog. Phys.* **55** 431–86
[14] Cox R G 1998 *J. Fluid Mech.* **357** 249–78
[15] Bertozzi A L 1998 *Not. Am. Math. Soc.* **45** 689–97
[16] Fisher L R and Lark P D 1979 *J. Colloid Interface Sci.* **69** 486–92
[17] Mann J A Jr, Romero L, Rye R R and Yost F G 1995 *Phys. Rev.* E **52** 3967–72
[18] Romero L A and Yost F G 1996 *J. Fluid Mech.* **322** 109–29
[19] Rye R R, Mann J A Jr and Yost F G 1996 *Langmuir* **12** 555–65
[20] Yost F G, Rye R R and Mann J A Jr 1997 *Acta Mater.* **45** 5337–45
[21] Rye R R, Yost F G and O'Toole E J 1998 *Langmuir* **14** 3937–43
[22] Darhuber A A, Troian S M and Reisner W W 2001 *Phys. Rev.* E **64** 031603
[23] Satoda Y and Ichikawa N 1994 *J. Colloid Interface Sci.* **162** 350–5
[24] Weislogel M M 1997 *AIChE J.* **43** 645–54
[25] 1996 *CRC Handbook of Chemistry and Physics* 77th edn ed D R Lide (Boca Raton, FL: CRC Press) pp **6-**147-**6-**148, **6-**208-**6-**209
[26] Hoffman R 1975 *J. Colloid Interface Sci.* **50** 228–41
[27] Schäffer E and Wong P-Z 1998 *Phys. Rev. Lett.* **80** 3069–72
[28] Schäffer E and Wong P-Z 2000 *Phys. Rev.* E **61** 5257–77
[29] Douglas J F 1969 *Introduction to Dimensional Analysis for Engineers* (London: Sir Issac Pitman and Sons) pp 116–17
[30] Szekely J, Neumann A W and Chuang Y K 1971 *J. Colloid Interface Sci.* **35** 273–8